ACS APPLIED ENGINEERING MATERIALS

pubs.acs.org/acsaenm Article

Crack Binding and Filling Properties of Modified Proteins in Sustainable Cementitious Materials

Elvis Baffoe and Ali Ghahremaninezhad*

Cite This: ACS Appl. Eng. Mater. 2023, 1, 2685−2697 Read Online

ACCESS | Metrics & More | Article Recommendations | Supporting Information

ABSTRACT: This study aims to investigate the effect of two modifying agents, sodium dodecyl sulfate (SDS) and lignin, on the properties of five different proteins and their crack binding and filling in the cementitious surface. The molecular structure and physicochemical properties of the modified proteins were examined using Fourier transform infrared (FTIR), differential scanning calorimetry, ζ-potential, and surface tension measurements. The binding between the modified proteins and the cementitious surface was evaluated using the interfacial shear lap test. The effect of the modified proteins on crack filling and healing of cementitious materials was studied by using flexural testing, optical microscopy, and X-ray microcomputed tomography. FTIR showed reduced intensities of the amide groups in the molecular structure of the modified proteins compared with the unmodified proteins. Proteins showed an increased viscosity in the synthetic pore solution (SPS) compared to that in deionized water, due to protein unfolding at a high pH of the SPS and subsequently cross-linking via Ca^{2+} bridging. Modifying with SDS generally increased the viscosity of the proteins due to increased cross-linking, while lignin did not seem to change viscosity. The proteins modified with SDS and lignin exhibited a general increase in interfacial shear strength between the modified proteins and the cementitious surface. It was found that modifying the protein sodium bovine immunoglobulin with SDS enhanced the crack healing and filling in cementitious materials, while modifying with lignin was not effective.

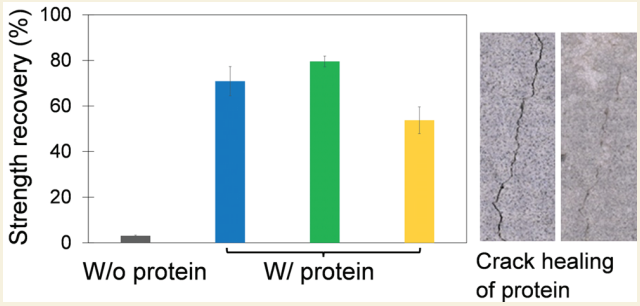

KEYWORDS: *proteins, self-healing, cementitious materials, sustainability, biocementation*

1. INTRODUCTION

Mother Nature has created biological composite materials, such as bone, nacre of abalone shell, and sea urchin, with superior mechanical and functional properties compared to synthetic materials.[1] This is a result of the interaction between the molecular and functional groups of certain biomolecules and inorganic materials.[2] The interaction between the biomolecules and the inorganic phase results in modification of the microstructure, which can lead to an enhanced macroscale performance of the biological composites.[3] Inspired by nature, there has been a spurt of research on exploiting biocementation in a wide array of applications such as improving the mechanical properties of porous materials,[4] enhancing the soil and sand performance,[5] increasing oil recovery,[6] and repairing concrete materials and limestone.[7,8]

Concrete is the most widely used man-made construction material with high compressive strength but low tensile strength.[7,9] The low tensile strength of concretes makes them susceptible to cracking.[10] Cracks in concrete serve as channels for harmful and deleterious substances to be transported into the concrete.[10] Consequently, these harmful substances may attack the steel reinforcement and reduce the long-term durability and performance of the concrete.[10] To address this problem, researchers have over the years investigated biocementation to repair cracks in concrete.[11] The biocementation process involves the precipitation of $CaCO_3$ by microorganisms to heal cracks in concrete and cementitious materials.[7,11]

Organic biomolecules, including proteins and polysaccharides, play an important role in the biocementation process. They provide a templating platform to control the nucleation, growth, and microstructure of the minerals.[12] Organic biomolecules can serve as an adhesive at the interface between mineral particles, imparting mechanical stiffness to sediments and precipitates.[13] A family of biomolecules, proteins, consist of amino acids with different functional groups including charged, hydrophobic, and hydrogen-bond-forming amino acids. The multitude of functional groups in proteins and their conformational structures provide a large variety of

Received: July 26, 2023
Revised: September 18, 2023
Accepted: September 20, 2023
Published: October 9, 2023

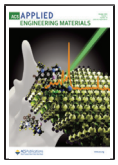

interaction pathways between proteins and solid surfaces.[14] Thus, due to the heterogeneity of surface characteristics of cementitious materials, proteins have the potential to interact with cementitious surfaces in a variety of ways. In a recent study,[15] it was indicated that the presence of organic matter was critical in providing binding and cohesion to loose sand treated with microbial-induced calcium carbonate precipitation. Their study showed that chemically synthesized calcium carbonate without the presence of organic matter was not able to consolidate the loose sands. Brzyski et al.[16] reported that the addition of casein protein improved the flexural strength of lime−metakaolin paste, which they attributed to increased interfacial strength between lime particles due to the presence of casein. Ventol et al.[17] demonstrated that the addition of adhesive protein enhanced the compressive strength and decreased the porosity of lime mortars. The interaction between proteins, amino acids, and calcium silicate hydrate, which constitutes the primary binding phase in cementitious materials was also examined by Kamali et al.[18] Prior studies investigated the properties of the proteins, bovine serum albumin (BSA) and human serum albumin, as binders in developing biocomposites for space construction applications.[19]

While the concept of biocementation for crack healing of cementitious materials has been extensively studied in the past,[7,11] the effect of organic biomolecules in the biocementation process for the crack healing of cementitious materials has not received attention and is not fully understood. Baffoe and Ghahremaninezhad[7] evaluated the influence of proteins on the biocementation process applied to loose ground-hardened cement paste powder and observed enhanced mechanical binding and lower porosity in the consolidated sample. Almajed et al.[20] also observed improved mechanical performance of consolidated loose sand treated with biocementation modified with casein protein. In a recent study, Baffoe and Ghahremaninezhad[9] investigated the influence of proteins on the crack healing of cement mortar samples. The researchers observed a 68% flexural strength recovery of cement mortars healed in protein solutions compared to cement mortars healed in water alone. The strength recovery improvement was attributed to the binding properties of the proteins and changes in the molecular structure of the proteins.

Several factors, including pH, ionic strength, denaturants, and additives, could modify the molecular structure of proteins and also influence their adhesive performance. Previous studies have shown that these factors can be exploited to engineer and improve the adhesive property of proteins in wood binding.[21,22] Sodium dodecyl sulfate (SDS) is an anionic surfactant and has been shown to enhance the interfacial adhesive in woods.[22] Lignin is the most abundant aromatic biopolymer and is derived from the industrial byproduct of pulping and biofuel production.[23] Previous investigations have indicated that lignin has the potential to improve the durability of soy protein adhesive.[21] In another study, the use of lignin was shown to enhance the binding strength and water resistance of protein adhesives.[24] The effect of the pH on the adhesive performance of lignin−protein adhesives was also evaluated in the past.[25] Via cross-linking with proteins, lignin improved the thermal stability, tensile strength, and Young's modulus of soy protein.[26]

Thus, motivated by the previous studies indicating the potential benefits of lignin and SDS in the adhesive performance and functionalities of proteins, our main goal of this paper was to elucidate the effect of SDS and lignin on the physicochemical properties of different proteins and their binding performance with a cementitious surface. To the best of our knowledge, this work is the first to examine the effect of lignin and SDS to tune and affect the adhesive properties of proteins in a cementitious environment. The use of lignin as a biomass byproduct in construction materials can contribute to the decarbonization and sustainability of the construction industry. Understanding the influence of protein molecular changes on cementitious materials can aid in laying the foundation for a new paradigm for employing engineered biomolecules to yield desired and enhanced functionalities in construction materials. The molecular structure of proteins was investigated by using Fourier transform infrared (FTIR) and differential scanning calorimetry (DSC). The effect of SDS and lignin on the surface tension and viscosity of the proteins was also investigated. The influence of SDS and lignin on the binding of proteins to cementitious surfaces and their crack-healing performance were investigated using the interfacial shear lap test, the three-point bend test, optical imaging, and X-ray microcomputed tomography (micro-CT).

2. EXPERIMENTS

2.1. Materials

2.1.1. Proteins and Modifying Agents. The proteins used consisted of whey protein, ovalbumin (albumin), nonfat milk diary powder (NFMP), sodium bovine immunoglobulin (SBI), and collagen peptide (CP). These proteins were purchased from commercial vendors. The native molecular structures of whey protein, albumin, NFMP, and SBI are reported to be globular, while CP is reported to have a fibrous structure.[27−29] The molecular weight and structure of these proteins have been studied in previous investigations.[3,7,30] The differences in the characteristics of these proteins and their availability are the reasons for including them in this study. Lignin is a hydrophobic phenolic compound found in biomass and possesses several functional groups including alcohol hydroxyl, phenol hydroxyl, and carboxyl groups capable of reacting with proteins to form protein−lignin complexes, hydrophobic networks, and hydrogen and ionic bonds.[31] SDS is an anionic surfactant composed of a hydrophilic 12-carbon chain tail and a hydrophilic sulfate headgroup.[32] The molecular structure of SDS enables SDS to react with proteins through its sulfate and alkyl chains.[33] Lignin and SDS were purchased from Sigma-Aldrich. The lignin used was an alkali lignin, which is produced using a sodium hydroxide solution at elevated temperature and pressure to break the linkages with polysaccharides.[34] The molecular weight of SDS was 288.38 g/mol.

2.1.2. Cement. A Type I/II ordinary Portland cement (OPC) was used in the preparation of the cement mortar prisms used in the interfacial shear strength test and crack-filling and healing tests. The chemical composition of the Type I/II OPC is shown in Table 1.

Table 1. Oxide Composition (%) of the Type I and II OPCs Used in This Study

CaO	SiO_2	Al_2O_3	Fe_2O_3	MgO	Na_2O	K_2O	SO_3	LOI	total
64	20.6	4.8	3.5	0.9	0.3	0.1	3.4	2.4	100

2.1.3. Synthetic Pore Solution (SPS). SPS was utilized in this study to evaluate the effect of high pH and ionic composition of the cementitious environment on the protein response. SPS was prepared to contain 0.02 M $Ca(OH)_2$, 0.037 M Na_2SO_4, 0.1062 M KOH, and 0.037 M K_2SO_4 following the procedure described in ref 35.

https://doi.org/10.1021/acsaenm.3c00423
ACS Appl. Eng. Mater. 2023, 1, 2685−2697

2.2. Methods

2.2.1. ζ Potential. The surface charge of the proteins and modifying agents, SDS and lignin, dissolved in SPS was measured using dynamic light scattering in a Zetasizer Nano ZS instrument (Malvern Instruments Ltd., Malvern, U.K.) conditioned at 25 °C. The refractive index and absorption coefficient for the analysis were set at 1.45 and 0.001, respectively. Approximately, 0.15% concentration of the proteins and modifying agents by mass of SPS was prepared and equilibrated for 10 min. The solutions were placed in a disposable folded capillary cell (DTS1070) and loaded into the instrument. The solutions were again equilibrated for 120 s before testing. Each sample was tested three times, and between each test, the data were collected after 100 or 110 runs.

2.2.2. Surface Tension. The surface tension of the protein solutions was measured to provide information about the surface hydrophobicity of the proteins. Solutions with protein concentrations of 0.12 g/mL and modified with SDS and lignin with concentrations of 1 M and 1% by mass of SPS, respectively, were prepared and allowed to equilibrate for 10 min. The surface tension values were measured by using a BZY 201 surface tension meter. Before each run, the ring was thoroughly heated by a wick flame and cleaned with acetone to remove organic contaminants. Three replicates were tested for each sample, and the average was reported.

2.2.3. FTIR. FTIR was employed to investigate the molecular structure of the modified proteins. To this end, solutions with a 0.12 g/mL concentration of proteins in four different media of deionized water (DW), SPS, SPS and SDS (SPS-SDS), and SPS and lignin (SPS-Lignin) were prepared, oven-dried at 50 °C for 24 h, and ground into fine powder. The concentrations of SDS and lignin added to the protein solutions to serve as modifiers were 1 M and 1% by mass of SPS, respectively. The powder samples were passed through sieve #60. Approximately, 30 mg of the sieved protein powder was utilized in the test. FTIR measurements were performed using a PerkinElmer Paragon 1000 FTIR spectrometer with an attenuated-total-refectance accessory in transmission mode. The scan resolution was 4 cm^{-1}, and the spectra were recorded between 600 and 4000 cm^{-1}. Each sample was taken through four scans, and an average of two samples from the four rounds of scans was reported for the analysis.

2.2.4. Viscosity. The viscosity of the protein solutions was measured using an NDJ-5S digital viscometer conditioned at 25 °C. The rotational viscometer worked by detecting the torque needed to rotate the rotor at a sustained speed while submerged in the protein solution. Based on the torque measurement, the fluid shear stress was found and the viscosity measured. Protein solutions with a volume of 25 mL and a concentration of 6% in DW, SPS, SPS-SDS, and SPS-Lignin were prepared. The concentrations of lignin and SDS used were 1% by mass of SPS and 1 M, respectively. The protein solutions were poured into a sleeve. The rotor #0 that is used to measure low-viscosity ranges was fixed to the viscometer, and then the sleeve was installed such that the rotor was just at the center of the opened sleeve. The rotor speed was set at 60 rpm. For each protein solution, three measurements were taken, and the average was reported.

2.2.5. DSC. DSC analysis of the proteins was performed with a PerkinElmer DSC 8500 instrument. First, proteins were dissolved in DW to achieve a protein concentration of 0.12 g/mL. The solution was oven-dried at 50 °C for 2 h to obtain a solid form. Approximately 5 mg of each sample was loaded into a stainless-steel pan and fitted with a stainless-steel lid. The sample was heated from 30 to 250 °C at a rate of 20 °C/min. Another stainless-steel pan fitted with a lid but without protein was placed side by side with the pan containing the protein to serve as a reference. The enthalpy of the proteins, peak area, and denaturation temperature were reported.

2.2.6. Interfacial Shear Strength. The interfacial shear strength between the cementitious surface and the modified proteins was evaluated by using the lap shear test. Cement mortar specimens used for the lap shear test were prepared by using a water/cement of 0.5 and a sand/cement of 2. The sand used consisted of fine quartz sand with a size in the range of 0.15−0.5 mm. The cement mortar was cast in a prismatic metallic mold with dimensions of 50 × 25 × 300 mm^3, covered with plastic sheets, and cured for 24 h. After 24 h, the prisms were demolded, wrapped in plastic bags to prevent moisture loss, and left to further cure in a humidity chamber (23 °C) until 28 days. The cement mortar pieces with dimensions of 50 × 25 × 25 mm^3 were cut from the prisms using a diamond saw and surface-polished using SiC paper with grit sizes of 320 and 500. Approximately 500 μL of 0.12 g/mL modified protein solutions was spread using a pipet over an area with dimensions of 30 × 25 mm^2 between two cement mortar pieces in a single lap mode, as shown in Figure S1. The modified protein solutions were prepared in SPS, SPS-SDS, and SPS-Lignin. The concentrations of SDS and lignin were 1 M and 1% by mass of SPS, respectively. The cement mortar pieces were pressed firmly together at the interface region with a rubber band and left to cure under ambient conditions for 72 h. Five replicates for each protein were tested and the interfacial shear strength σ_s was calculated by eq 1 as follows:

$$\sigma_s = \frac{N_{max}}{A_b} \tag{1}$$

where N_{max} is the maximum shear load (N) attained before failure and A_b is the surface area of the interface region (mm^2).

2.2.7. Flexural Strength Recovery. Cement mortar prisms with dimensions of 150 × 55 × 25 mm^3, a water/cement of 0.5, and a sand/cement of 2 were cast and cured for 52 days. A notch with a width and length of 2 and 14 mm, respectively, was introduced in the middle of the top surface of the prisms using a diamond saw. The prisms were loaded into the three-point bend mode setup as shown in Figure S2 to grow a single crack with a crack mouth opening displacement (CMOD) of approximately 100 μm after unloading. The CMOD was monitored using an extensometer attached to two small metal plates close to the notched area. The two metal plates served as contact points for the pins of the extensometer because the notch width was too small to accommodate the pins of the extensometer. Loading was performed using an Instron testing machine at a displacement rate of 0.005 mm/s. The test was done using only SBI protein with a 3% concentration in SPS, SPS-SDS, and SPS-Lignin. SDS and lignin with a concentration of 1 M and 1% by mass of SPS, respectively, were added to the SBI protein in SPS. These concentrations were selected so as to achieve adequate solubility. The solution was then transferred into an open container for wet/dry cycle healing. The control cracked sample was healed using SPS. The healing procedure consisted of partially submerging the cracked prisms in the respective solutions for 3 h (wet cycle) and exposing them to ambient conditions for 21 h (dry cycle). On the seventh day, the prisms were left to dry in ambient conditions for an additional 48 h, and then their surfaces were imaged for crack-filling examination. The images of the cracked prisms after the healing process were compared with the images of the cracked prisms before healing. Then, the prisms were loaded into a three-point bend mode until complete failure. Three replicates for each protein solution were tested, and the average was reported. The flexural strength recovery ratio of each healed prism was determined using eq 2:

$$\text{flexural strength recovery (\%)} = \frac{P_{max,reloading} - P_{unloading}}{P_{max,uncracked} - P_{unloading}} \tag{2}$$

where $P_{max,reloading}$ is the maximum load obtained after healing, $P_{max,uncracked}$ is the maximum load of the uncracked sample, and $P_{unloading}$ is the residual load obtained before unloading. This corresponds to the load at which the prisms were unloaded during the initial crack generation.

2.2.8. Micro-CT Analysis. The crack filling of the cracked cement mortar prisms was evaluated using micro-CT. Micro-CT is valuable for providing information about internally formed cracks that are sometimes not visible to surface optical imaging. The cracked prisms before and after healing were scanned for comparison. Before the healed prisms were scanned, they were oven-dried at 54 °C for 24 h to remove moisture. The imaging was performed using a Bruker SkyScan 1273 (Bruker, Kontich, Belgium) at a scanning resolution of 27 μm/

https://doi.org/10.1021/acsaenm.3c00423
ACS Appl. Eng. Mater. 2023, 1, 2685−2697

pixel and with a 2 mm copper filter. The exposure time, average frame, rotational step, voltage, and current were 4350 ms, 10, 0.5°, 130 kV, and 115 μA, respectively. The cement mortar prisms were held firmly in a polyethylene container filled with styrofoam. The prisms were positioned between an X-ray source and a detector and scanned for a period of about 5 h, during which about 380 projections over 180° were taken. 3D reconstruction and quantification of the images were performed using *CTAnalyzer* software (1.20.8). The prisms were segmented into solid matrixes and voids using the gray-scale intensity thresholds, with the gray-scale range of 0−70 representing the voids.

3. RESULTS AND DISCUSSION

3.1. ζ Potential

The ζ potential measures the surface charge of colloidal particles and, in turn, determines the electrostatic interaction between them.[36] It provides an understanding of the stability of the colloidal system.[37] A high negative or positive ζ-potential value shows an adequate electrical double-layer repulsion between the colloidal particles, which inhibits their aggregation.[38] In this study, the effect of SPS with a high pH of 13.6 and ionic strength on the charge of the proteins and the modifying agents, SDS and lignin, was studied.

The ζ potentials of the proteins and the modifying agents, SDS and lignin, in SPS are shown in Figure 1. Generally, it is

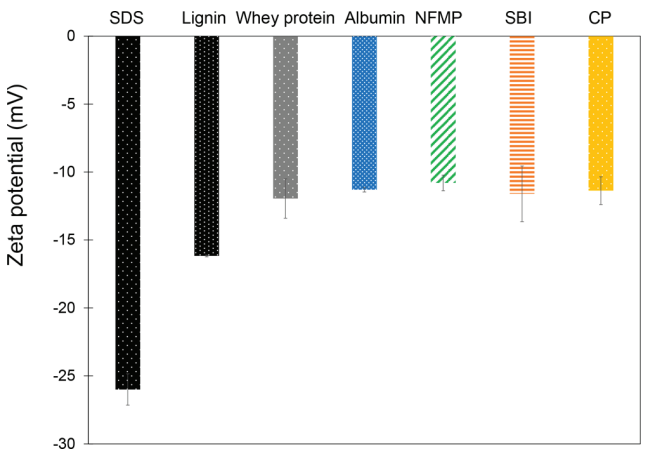

Figure 1. ζ potentials of SDS, lignin, and the proteins in SPS.

seen that SDS, lignin, and proteins in SPS exhibited negative charges, with SDS exhibiting a relatively higher negative charge of −26 mV. Lignin exhibited a negative charge of about −16.6 mV, while the maximum negative charge exhibited by the proteins was about −11.95 mV due to deprotonation of the amino acids of the proteins.[9] The negative charge exhibited by SDS is due to the presence of a sulfate functional group within the structure of SDS.[39] The negative charge of the lignin is a result of the negatively charged phenols.[38]

In a high-pH solution, the conformational and molecular structure of the proteins change through the breakage of hydrogen, hydrophobic, van der Waals, and disulfide bonds. Compared to other studies,[3,9] it was noticed that the negative surface charge exhibited by the proteins in this study is relatively low. The charge-screening effect due to the presence of Ca^{2+} in SPS and the formation of complexes and agglomerates results in a lower negative charge of the proteins. The negative functional groups of SDS and lignin can form complexes with divalent cations, and this is suggested to be the reason why these modifiers exhibited relatively a lower negative charge compared to what is reported in the literature.[39]

3.2. Surface Tension

Figure 2 shows the surface tension of the proteins in SPS, SPS-SDS, and SPS-Lignin. The measurements were taken twice in

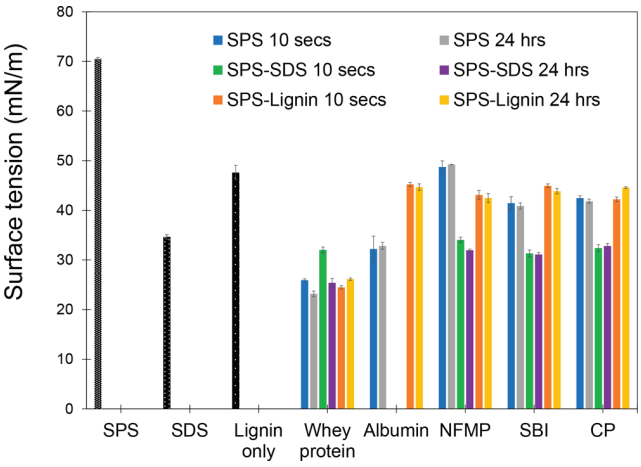

Figure 2. Surface tensions of the proteins in SPS, SPS-SDS, and SPS-Lignin.

24 h: immediately after mixing and 24 h after mixing. This was done to study the time-dependent effect of the pH, Ca^{2+}, and modifying agents on the surface tension of the proteins. The surface tension of albumin in SPS-SDS could not be measured due to the high stiffness of the resulting gel. Generally, it was noticed that the proteins exhibited different surface tension results. Whey protein exhibited the lowest surface tension in all media, which is an indication of a higher content of hydrophobic groups in whey protein.[3,9] While albumin in SPS showed a lower surface tension compared to those of NSMP, SBI, and CP, in SPS-Lignin, these proteins had similar surface tensions. The pH of the solutions was measured to be above 13. Because this pH is above the isoelectric points of the proteins, the proteins may undergo molecular and conformational changes and begin to unfold to expose their hydrophobic groups.[7] It is seen that generally the surface tension of the proteins did not vary with time; that is, the surface tension remained similar throughout the 24-h period. The relatively lower surface tension of the proteins in SPS-SDS is largely contributed by the hydrophobicity of the SDS because reports indicate that SDS is hydrophobic in nature.[31,32] The surface tension of the proteins in SPS-Lignin appeared to be higher than the surface tension of the proteins in SPS, which is due to the higher surface tension of lignin compared to the proteins. The extent of the changes in the molecular structure of the proteins and the number of hydrophobic groups in individual proteins are responsible for the variation in the surface tension, as depicted in Figure 2.

3.3. FTIR

The FTIR spectra of the modified proteins were obtained to evaluate the changes in the molecular structure of the proteins in SPS, SPS-Lignin, and SPS-SDS compared to that in DW. It is known that proteins denature and aggregate at high pH and in denaturing solutions. Also, proteins are likely to interact with ions, especially Ca^{2+}, via cross-linking.[40] As shown in Figure 3, the spectra showed typical peaks corresponding to

https://doi.org/10.1021/acsaenm.3c00423
ACS Appl. Eng. Mater. 2023, 1, 2685−2697

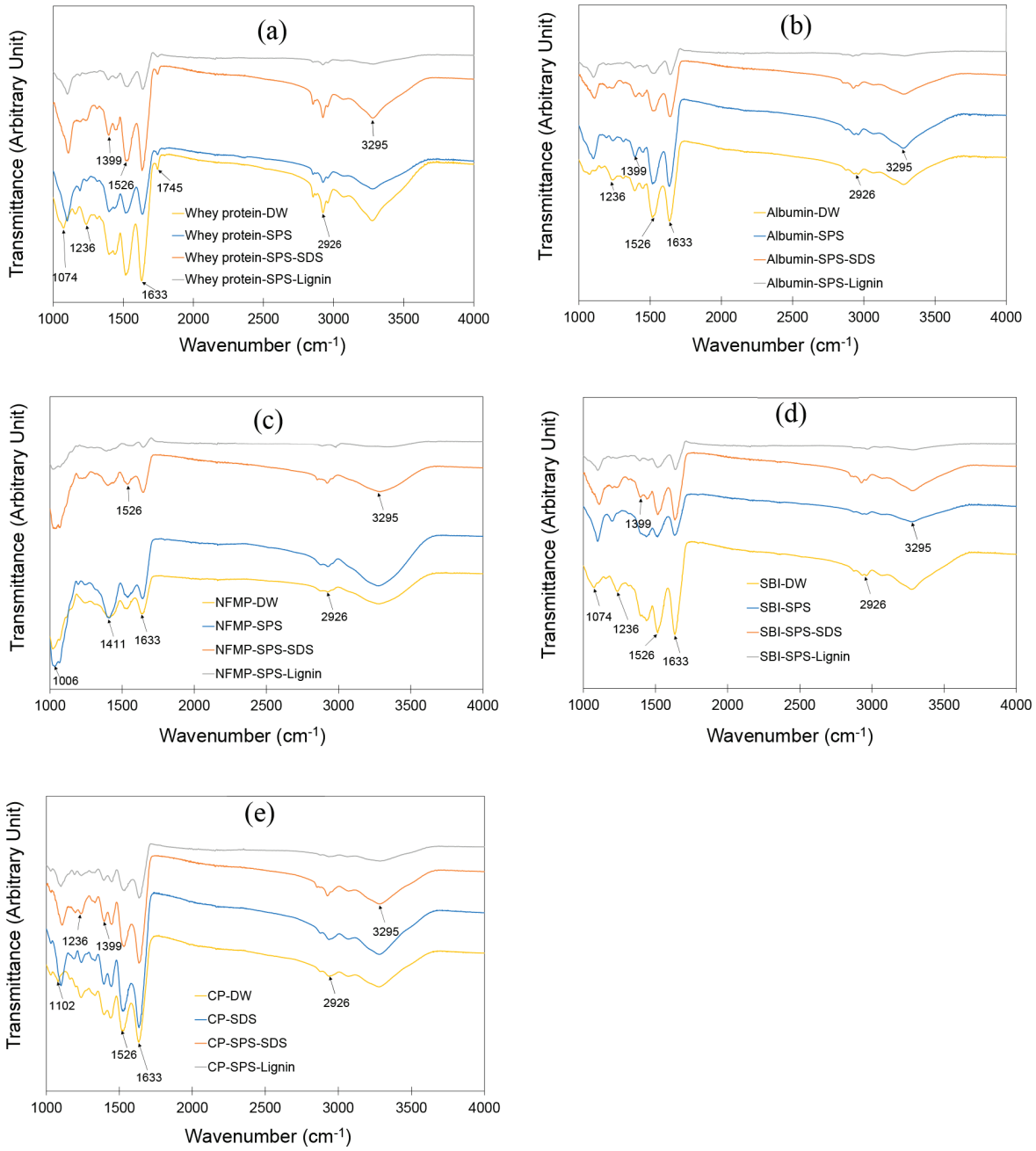

Figure 3. FTIR spectra of (a) whey protein, (b) albumin, (c) NFMP, (d) SBI, and (e) CP in DW, SPS, SPS-SDS, and SPS-Lignin.

proteins, as identified by the presence of amide I, amide II, and amide III at 1633, 1526, and 1236 cm^{-1}, respectively.[41] Amide I represents the C═O stretching vibration of the peptide group of the protein. Amide II and amide III are assigned to the N−H bending with a contribution from C−N stretching vibrations and C−N and N−H, respectively.[41] Generally, it is seen that whey protein and SBI showed some reduction in the intensity of the peaks associated with amide I and amide II in SPS. This is possibly attributed to the interaction between Ca^{2+} and the NH, C═O, and COO− groups of whey protein and SBI resulting in a reduction of the α-helix structure.[42]

The peak corresponding to amide III (1236 cm^{-1}) either disappeared, shifted to lower wavenumbers, or were weaker in the proteins modified in SPS, particularly whey protein, albumin, and SBI. The amide III peak shows more distinct secondary structures of proteins and as such has been used to evaluate the secondary molecular structure of proteins.[43,44] The observed reduction in intensity, disappearance, or shift in the peak of amide III correspond to the denaturation of the proteins[44] due to the high pH level of the SPS. The proteins modified in SPS-Lignin showed a decreased peak at 1399 cm^{-1}, indicating that the COO− group of the proteins served as an active group and interacted with lignin.[21] It was also noticed that the addition of lignin led to the complete hydrolysis of the molecular structure of NFMP, and this was shown by the complete disappearance of all of the functional peaks. This lignin-induced hydrolysis seemed to occur to different extents in the other proteins.

Noticeably, a common peak appeared at about 2926 cm^{-1}. This peak corresponds to the C−H stretching vibration of CH_2

https://doi.org/10.1021/acsaenm.3c00423
ACS Appl. Eng. Mater. 2023, 1, 2685−2697

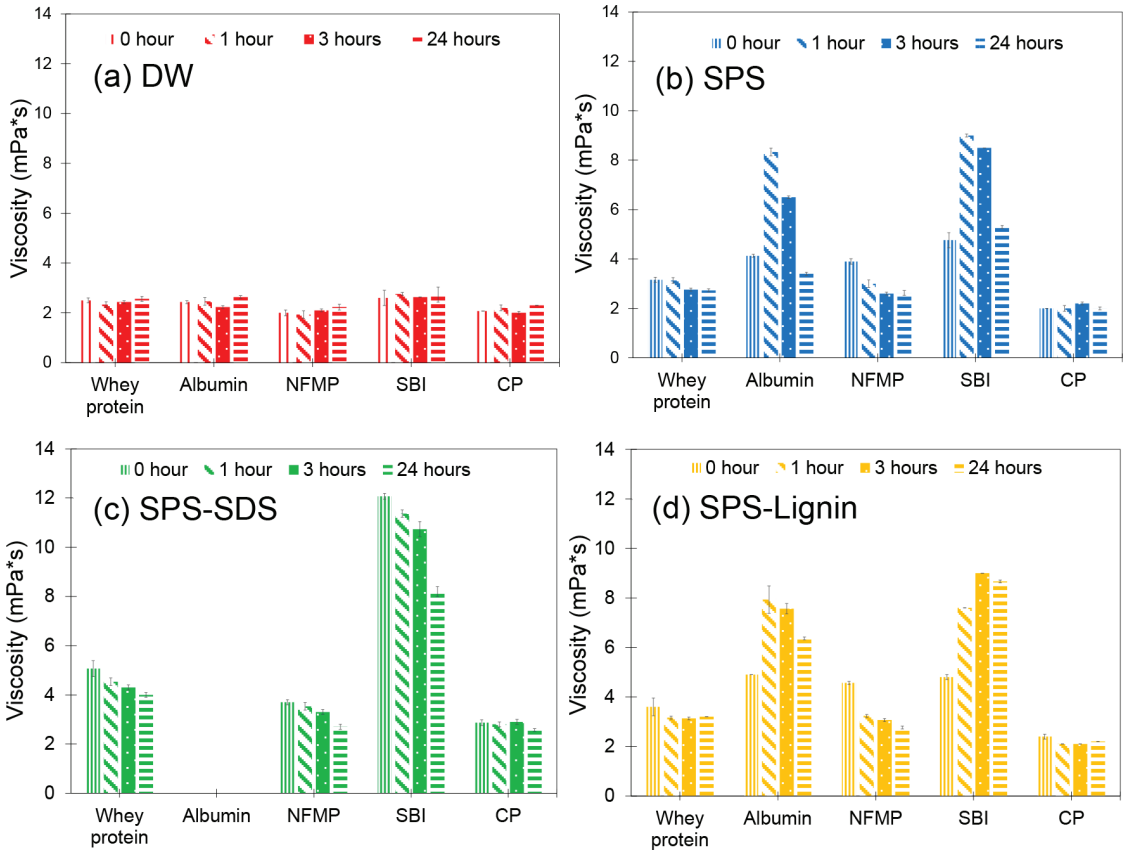

Figure 4. Viscosity of the proteins in (a) DW, (b) SPS, (c) SPS-SDS, and (d) SPS-Lignin.

and CH_3 of the proteins, which is situated at the hydrophobic side chain of the proteins.[45−47] It is worth noting that the assigned hydrophobic peak was most pronounced in whey proteins in DW, which corresponds to the natural protein natural state. This supports the observation made in the surface tension results in Figure 2 that, among the proteins, whey protein had more hydrophobic groups, as demonstrated by a lower surface tension compared to other proteins. It is also interesting to note that the peak intensity at 2926 cm^{-1} for the proteins reduced in SPS. It is possible that, due to the high pH level of SPS, continuous denaturation of the protein might have led to an aggregation, which might have reduced the hydrophobicity of the protein. In SPS-SDS, it was noticed that the amide and hydrophobic peaks exhibited slightly stronger intensities compared to those in SPS, and that was due to the presence of SDS.[31,32] This is in support of the surface tension results, where proteins in SPS-SDS showed higher hydrophobicity. According to the literature, the peak at 1745 cm^{-1} for whey protein is associated with ester linkage.[48,49] This peak is an intermolecular covalent bond formed between the side chains of Thr−Gln amino acids in whey protein.[50]

The peaks located at 1399 and 1074 cm^{-1} can be assigned to the stretching vibrations of COO− and C−O of the hydroxyl group bound to carbon.[48] The shift of the C−O peak assigned at 1074 cm^{-1} to about 1101 cm^{-1} in the spectra of all proteins in SPS, SPS-SDS, and SPS-Lignin may be an indication of cross-linking.

3.4. Viscosity

The viscosity of the proteins in different media was measured as a function of time to understand the effect of protein unfolding and cross-linking on their viscosity. The viscosity of the protein solution can be affected by many factors such as the molecular weight and shape, flexibility, intermolecular interactions, pH, viscosity of the solvent, shear rate, surface charge, and ionic concentration.[51] The values of the viscosity are plotted against time in Figure 4. It is seen in Figure 4a that the viscosity of the protein solutions largely remained unchanged throughout the time in DW. The higher viscosity of the proteins, especially albumin and SBI, in SPS, as seen in Figure 4b, may be attributed to the cross-linking between Ca^{2+} and the protein molecules. Ca^{2+} can act as a cross-linker in protein solutions. When a protein is mixed with Ca^{2+}, calcium bridges are formed between the protein molecules. The calcium bridges formed lead to the formation of a 3D protein network[52] which makes the resulting protein solution more viscous. The formation of a viscous protein solution due to Ca^{2+}−protein molecule interaction is in agreement with that in previous studies.[53] In addition, the effect of high pH can have a significant influence on the viscosity of a protein solution. The pH level investigated in this study causes partial unfolding of the protein molecules, exposing the hydrophobic and hydrophilic residues. The exposed hydrophilic residues interact with the surrounding water molecule to form hydrogen bonds, which subsequently increases the viscosity of the resulting solution.[54]

In SPS-SDS, it was noticed that the viscosity of the protein solutions was higher compared to that in DW, SPS, and SPS-Lignin, and this was more noticeable in the case of whey protein, albumin, and SBI. The reason for the higher viscosities in SPS-SDS can be attributed to the formation of a gel-like phase as a result of the cross-linking interaction among the

https://doi.org/10.1021/acsaenm.3c00423
ACS Appl. Eng. Mater. 2023, 1, 2685−2697

proteins, SDS, and Ca^{2+}. As shown in Figure 1, both the protein and SDS are negatively charged. The presence of Ca^{2+} in the solution can facilitate cross-linking among molecules of both the negatively charged proteins and SDS and form a gel-like molecular network.[9] The formation of protein−surfactant gels due to the interaction between BSA and SDS has been investigated by Roversi and La Mesa.[55] A complete transformation of albumin in SPS-SDS into a gel made it difficult to measure the viscosity of the albumin. Lignin has a phenol group and is able to form cross-links with proteins[56] and interact with proteins to form protein−lignin complexes by hydrophobic interactions and ionic hydrogen bonds similar to the interactions between proteins and polyphenol.[31] Thus, the interaction between the lignin and proteins increases the viscosity of the solution.[31] However, the proteins exhibited similar viscosity values in SPS and SPS-Lignin, indicating that the change in the molecular structure of the proteins in SPS-Lignin did not noticeably affect the viscosity compared to that in SPS.

3.5. DSC

A DSC experiment was carried out to investigate the enthalpy of the protein denaturation due to the thermal effect.[27] Previous studies have reported that the characteristic of proteins during heating is associated with a change in the protein thermal property.[57] The enthalpy changes that result from protein unfolding correspond to the extent of denaturation and can be studied using DSC.[58] From Figure 5, it can be seen that all of the proteins showed broad endothermic peaks between 70 and 120 °C. SBI and albumin showed additional peaks at 220 and 213 °C, respectively.

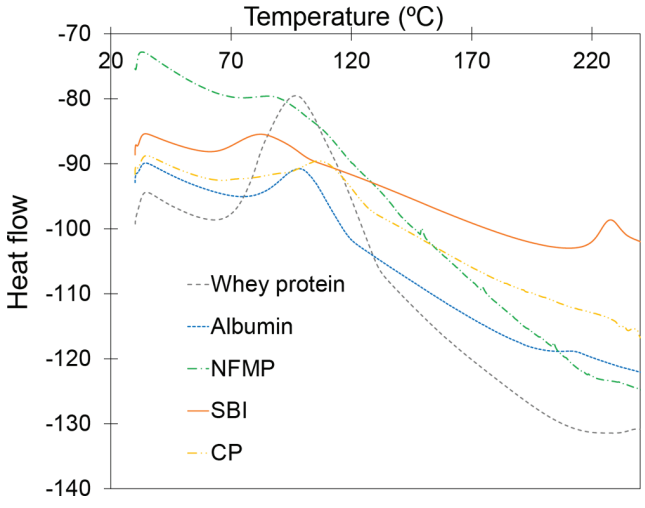

Figure 5. DSC results for the proteins in DW.

The enthalpy values (ΔH) obtained for whey protein, albumin, NFMP, SBI, and CP were 167, 110, 112, 237, and 79 J/g, respectively, as shown in Table 2. During protein denaturation, ΔH is associated with the interruption of van der Waal and hydrogen bonds in the internal structure of protein and water.[59] Patel et al.[60] reported that ΔH is in agreement with the ordered secondary structure of proteins and can provide insight into the fraction of undenatured proteins. Denatured proteins have been reported to possess lower ΔH due to the destruction of hydrophobic bonds.[57] From the test result, the apparent higher ΔH of whey protein

Table 2. DSC Thermal Characteristics of the Proteins in DW

protein	ΔH (J/g)	area (mJ)
whey protein	167	2342
albumin	110	767
NFMP	112	630
SBI	237	1328
CP	79	582

and SBI is attributed to the amount of energy consumed to break the hydrophobic bonds present in the structure of whey protein and SBI.[27] Because whey protein in its native state possessed more hydrophobic bonds than the other proteins, more energy would be required to break these hydrophobic bonds. In addition, individual globular proteins such as bovine β-lactoglobulin, bovine α-lactalbumin, BSA, and immunoglobulins that constitute the molecular structure of whey protein are hydrophobic[27] and may consume higher energy to break the bonds. It is interesting to note that immunoglobulins are part of the molecular structure of SBI.

According to the results shown in Table 2, CP showed the lowest ΔH and area of decomposition, and this may be attributed to the reduced hydrophobic bonds in the CP protein, as indicated by their surface tension results. It is seen that SBI and albumin showed additional peaks at higher temperatures. These additional peaks may correspond to stronger bonds that require higher energy levels to break.

3.6. Interfacial Shear Strength

The interfacial shear strength between modified proteins and the cement mortar surface is illustrated in Figure 6. The

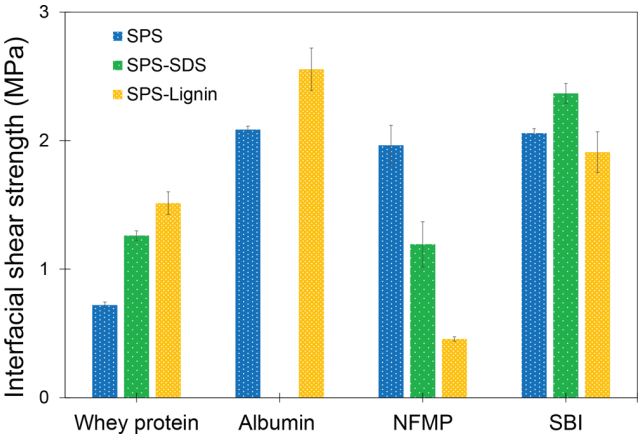

Figure 6. Interfacial shear strength between the cement mortar surface and proteins modified in SPS, SPS-SDS, and SPS-Lignin.

interfacial shear strength of the cement mortar surface and albumin in SPS-SDS was not determined because the solution was highly viscous and could not be spread on the surface of the cement mortar prism. The properties of polymers such as the functional group, viscosity, molecular weight, etc., are important factors that influence the interfacial shear strength between cement paste and polymers.[61] A previous investigation showed that the interfacial shear strength between the proteins and cementitious surface increased in SPS compared to that in DW.[9] From Figure 6, it is seen that the interfacial shear strength of the cement mortar surface and proteins in SPS-SDS and SPS-Lignin was generally higher compared to

https://doi.org/10.1021/acsaenm.3c00423
ACS Appl. Eng. Mater. 2023, 1, 2685−2697

samples with proteins in SPS only, except in the case of the cement mortar prisms with NFMP, where NFMP in SPS showed a higher interfacial shear strength than NFMP in SPS-SDS and SPS-Lignin. The improved interfacial binding of the proteins in the presence of lignin and SDS is comparable to the results of the prior literature.[21,22] The increase in the interfacial shear strength of cement mortar prisms with proteins in SPS-SDS is attributed to the formation of gels due to the interaction among Ca^{2+}, proteins, and SDS.[55] An investigation by Hansen et al.[33] indicated that negatively charged SDS binds strongly to cations and the hydrophobic amino acids of proteins through their alkyl and sulfate groups. The interaction between the functional groups of the proteins and the active groups of the modifying agents can lead to the formation of cross-linked networks that improve the interfacial bond between the proteins and cement mortar surface. The cross-linked network between soy protein and lignin was reported in prior investigations.[31,56] The hydrophobic and hydrophilic domains of the proteins enable the proteins to interact strongly with lignin.[62]

As noted previously, NFMP in SPS-SDS and SPS-Lignin showed a lower interfacial shear strength than those modified in SPS. The observed lower interfacial shear strength may be attributed to the hydrolysis of NFMP in these solutions, resulting in the breakdown of bonds and reducing the molecular weight, thus rendering the denatured NFMP protein ineffective in forming an adhesive bond with a cement mortar surface. This behavior is consistent with the FTIR results where it was shown that all of the major functional groups of NFMP completely disappeared in SPS-Lignin. A similar behavior of NFMP hydrolysis has been observed in prior studies.[9]

3.7. Flexural Strength Recovery

Figure 7 shows the flexural strength recovery of cracked cement mortar prisms. SBI modified in SPS, SPS-SDS, or SPS-Lignin was used for the healing solution of the cracked prisms. The reason for selecting SBI in the flexural strength recovery test was because it showed a relatively higher interfacial shear strength compared to that of the other proteins. The control cement mortar prisms were healed in SPS. It can be seen that the cement mortar prisms healed in SPS showed significantly lower flexural strength recovery compared to the prisms healed in SBI-SPS, SBI-SPS-SDS, or SBI-SPS-Lignin. The low flexural strength recovery exhibited by the control prism may be attributed to autogenous healing as a result of the hydration of the unreacted cement clinker and $CaCO_3$ formation.[7] A similar flexural strength recovery was observed in a previous study by Baffoe and Ghahremaninezhad.[9] It must, however, be mentioned that the healing solution used in the previous study was DW.

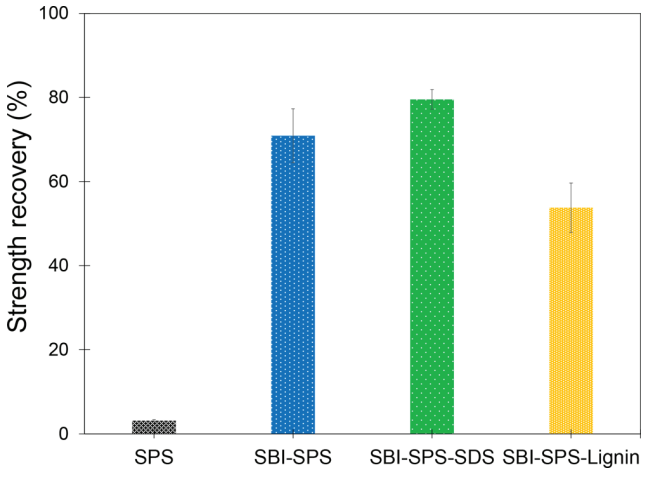

Figure 7. Flexural strength recovery of cracked cement mortar prisms healed in different protein solutions.

Cracked cement mortar prisms healed in either of the SBI modified solutions showed a significant flexural strength recovery. Comparing the above results with the prior studies[63,64] indicates the potential of proteins to significantly improve the mechanical recovery strength in cementitious materials. It should, however, be kept in mind that other factors, including the mix design and healing process, could also affect the performance of the proteins. The higher flexural strength recovery in these samples compared to the control can be attributed to the higher molecular weight and the ability of the SBI to adsorb onto the cement mortar surface and self-assemble to form a bond line, which could potentially enhance the interfacial bonding between the crack surfaces.[9] SBI has been reported to have a significant portion of protein of about 90%[65] and a molecular weight of about 160 K g/mol,[9] which is significantly higher than most proteins.[66] This demonstrates higher amino acid side chains in the molecular structure of SBI that could potentially lead to the formation of several cross-link networks and entanglements capable of increasing the number of bonds. Increased bond formation could increase the stiffness of the protein and subsequently increase the interfacial shear strength. In addition, the higher amino acid chain length in the molecular structure of SBI may provide greater cohesiveness between protein−protein interactions, which may allow elongation prior to their breakage.

The presence of Ca^{2+} in the healing media promotes cross-linking between the proteins and Ca^{2+} in SPS, as revealed in Figure 4, thereby increasing the protein−protein interactions and consequently enhancing the strength recovery of the cracked prisms healed in SBI-SPS. The role of Ca^{2+}−protein complexation in improving the mechanical binding between loose sand particles was also pointed out in a prior study.[67] In addition, the increased contact area between the cracked area and SBI due to exposure of the hydrophobic and hydrophilic groups of SBI may be one of the reasons for the higher flexural strength recovery of the healed cracked prisms.[9] It was shown in a prior study that the change in the molecular structure of the proteins as a result of denaturation leads to an increase in the contact area and binding between the protein and other surfaces.[68]

The flexural strength recovery results seem to be consistent with the interfacial shear strength results involving SBI, as discussed in Figure 6. It is seen that the samples healed in SBI-SPS-SDS showed the highest strength, averaging 80%. SDS is an anionic molecule[32] with a negative charge, as revealed by the ζ potential results in Figure 1. Therefore, SBI and SDS are expected to interact via Ca^{2+} bridging due to the presence of Ca^{2+} in SPS and of hydrophobic moieties.[33] The partial denaturation of SBI in SPS-SDS exposes the secondary structures of SBI and increases the contact area and adhesive force between the partially unfolded protein and the crack surfaces to ensure a higher bond strength.[22] The SBI-SPS-Lignin healed samples showed slightly lower strength recovery possibly due to excessive degradation of the molecular structure of SBI, as revealed in the FTIR results shown in

https://doi.org/10.1021/acsaenm.3c00423
ACS Appl. Eng. Mater. 2023, 1, 2685−2697

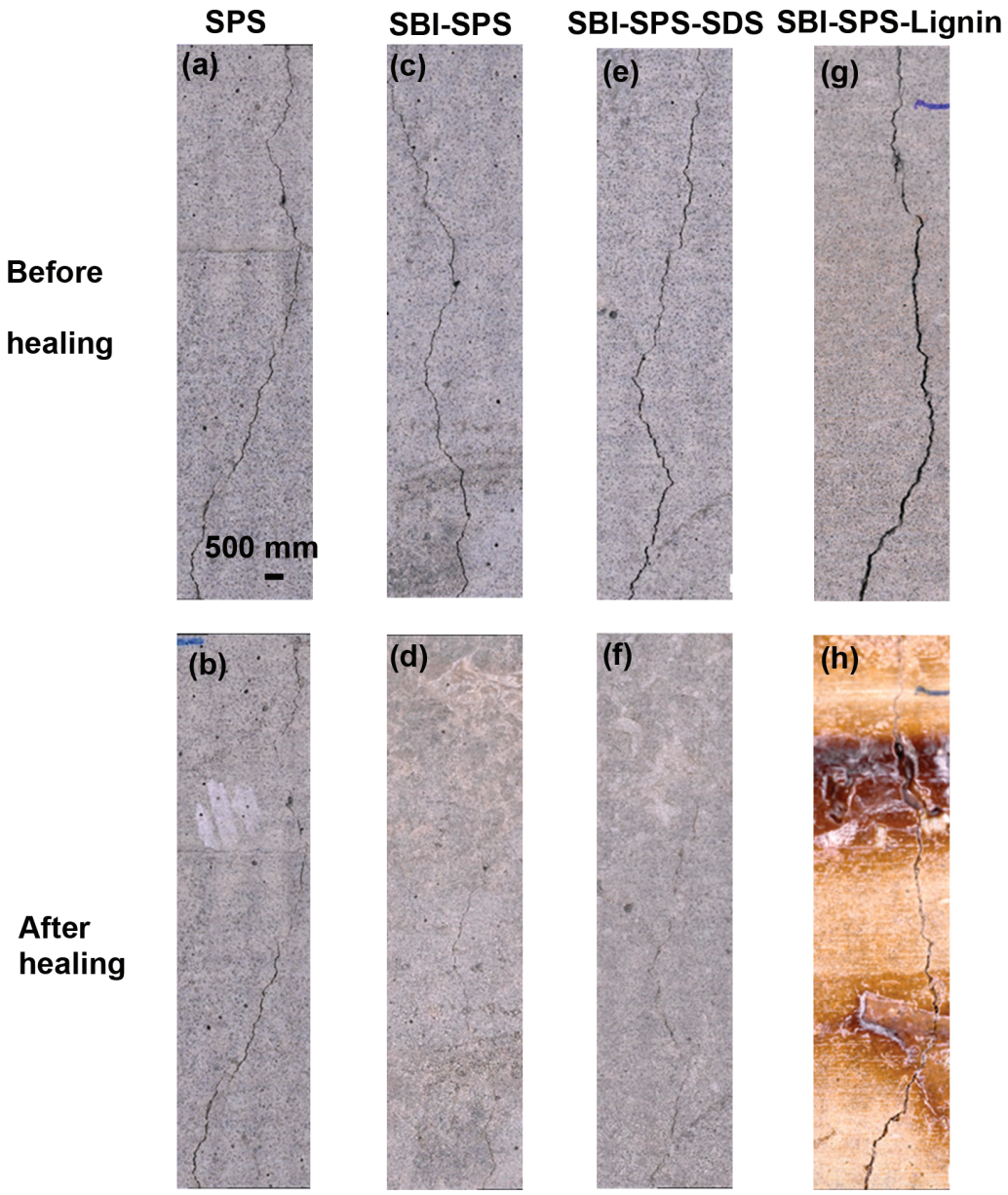

Figure 8. Images of the cement mortar prisms showing the crack filling of samples (a, c, e, and g) before and (b, d, f, and h) after healing. The scale bar is the same for all images.

Figure 3. This indicates that the 1% lignin concentration was not the optimum concentration of lignin. Further research is needed to examine the effect of lignin concentrations on the interfacial shear strength and strength recovery of cracked cement mortar surfaces.

3.8. Crack Closure

The crack closure ability of the cracked cement mortar prisms healed in SPS, SBI-SPS, SBI-SPS-SDS, and SBI-SPS-Lignin after 7 days of wet−dry healing cycles is illustrated in Figure 8. It is seen that the cement mortar prisms healed in the various solutions showed partial or complete crack closure after 7 days of healing. The control prism (SPS healed) shown in Figure 8b exhibited partial crack closure. The partial crack closure for the control prism is attributed to autogenous healing, which comes about as a result of the hydration of unreacted cement clinkers and carbonation of CH.[9] It is observed that the cracked cement mortar prisms healed in the SBI-SPS solution in Figure 8d showed a complete crack closure after the healing period. This is consistent with the observation made in our previous study[9] and corresponds to the higher flexural strength recovery observed in Figure 7. SBI has a higher affinity toward hydrated cement paste, as revealed in a previous study,[7] and can effectively adsorb onto the cracked cement paste, self-assemble, and form a gel to bind the crack surfaces together. Cement mortar prisms healed in SBI-SPS-SDS, shown in Figure 8f, also exhibited complete crack closure. This can be attributed to the adsorption and increased contact area of the partially unfolded proteins facilitating the interaction between the cracked surfaces and proteins. The cement mortar prism healed in SPS-SBI-Lignin showed partial crack filling, as demonstrated in Figure 8h. However, crack filling was less effective compared to the prism healed in SPS-SBI and SPS-SBI-SDS; this observation seems to be in agreement with the flexural strength recovery results discussed in Figure 7. It appears that

https://doi.org/10.1021/acsaenm.3c00423
ACS Appl. Eng. Mater. 2023, 1, 2685−2697

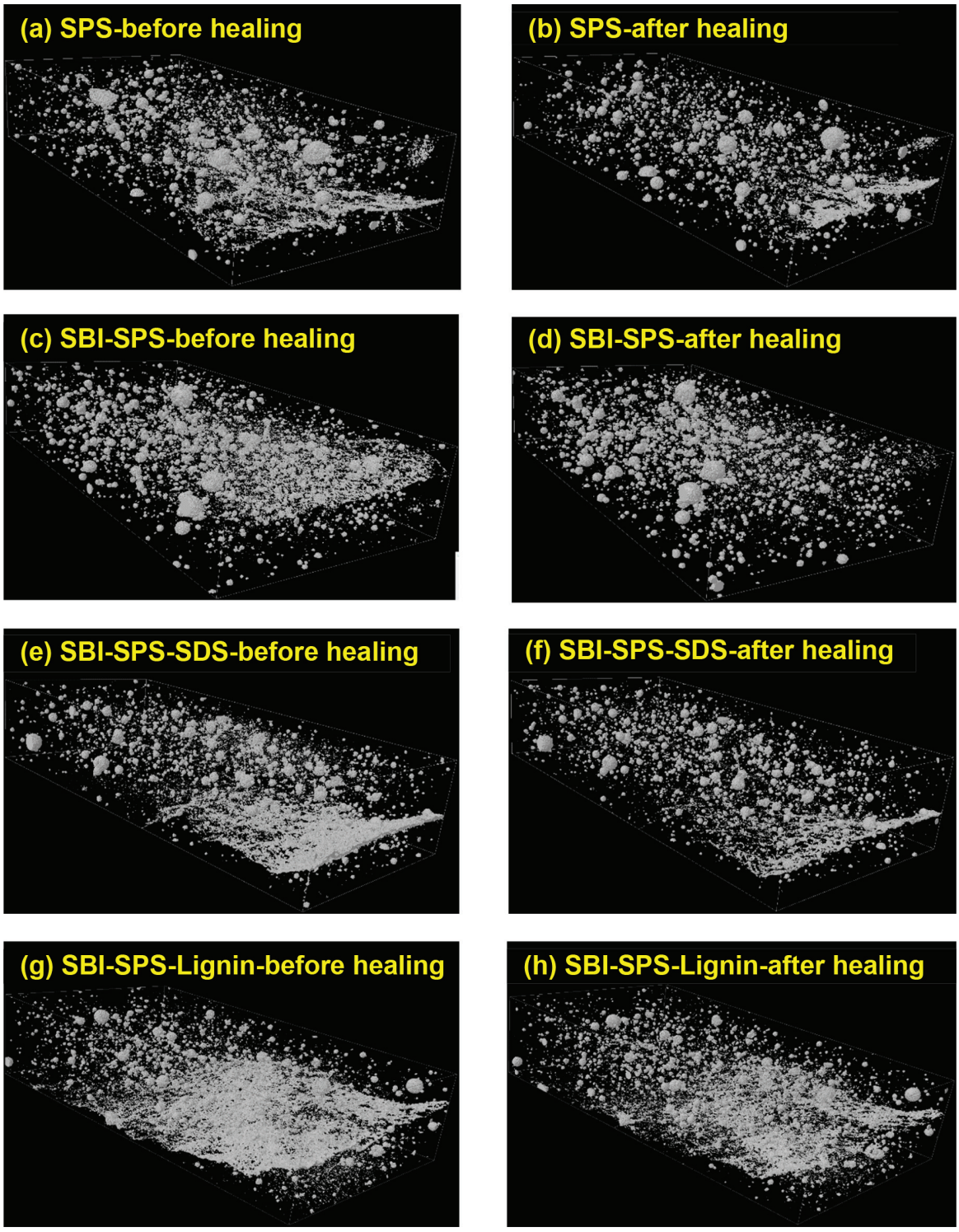

Figure 9. Micro-CT images illustrating empty spaces (voids and cracks) in the section near the crack in the cement mortar prisms (a, c, e, and g) before and (b, d, f, and h) after healing in different healing solutions.

the change in the molecular structure of SBI in SP-Lignin resulted in inadequate adsorption of SBI onto a cracked cement paste surface and less compact healing products in the crack space. It should be noted that the crack width in the prism healed in SBI-SPS-Lignin seemed to be slightly larger than that in the prisms used in other solutions despite using the same method of creating the initial cracks. This larger crack width could potentially contribute to a lower crack filling in this prism.

3.9. Micro-CT Analysis

A schematic depicting the sections of the prisms used in micro-CT analysis is shown in Figure S3. Figure 9 illustrates the 3D reconstruction of the internal microstructure of the cracked prisms near the crack before and after the healing cycles. The

https://doi.org/10.1021/acsaenm.3c00423
ACS Appl. Eng. Mater. 2023, 1, 2685−2697

empty spaces including voids and main cracks are represented in a gray color. The filling of the crack after the healing cycles is shown by a reduction in the volume of the gray features. It is seen that the cracked cement mortar prism healed in SPS showed a reduction in the volume of the gray features, demonstrating autogenous healing of the cracks after the 7-day healing period, as observed in Figure 9b. The cement mortar prism healed in SBI-SPS (Figure 9d) showed an enhanced filling of the crack, as demonstrated by the disappearance of the gray features near the crack. The SBI-SPS-SDS healed cement mortar prisms also showed noticeable crack filling, consistent with the optical imaging depicted in Figure 8f. Among the samples, the SBI-SPS-Lignin healed prism (Figure 9h) showed less crack filling compared to that of prisms healed in other solutions. The observations from micro-CT seem to be in good agreement with the results obtained from the optical imaging discussed in Figure 8.

4. CONCLUSIONS

In this study, the effect of two modifying agents, SDS and lignin, on the properties of five different proteins and their crack binding and filling in cementitious materials was investigated. Proteins reduced the surface tension of SPS due to unfolding and exposure of the hydrophobic functional groups in their molecular structure. The addition of SDS reduced the surface tension of the proteins due to a low surface tension of SDS in SPS. Lignin did not lower the surface tension of the proteins in SPS. The results from FTIR analysis indicated decreased intensities of amides I–III of the proteins in SPS and SPS-SDS due to the high pH and ionic interactions. In SPS-Lignin, these functional groups reduced the intensity, and in the case of NFMP, these functional groups disappeared. The viscosity of the proteins increased in SPS compared to that in DW due to denaturation of the proteins and the interaction between Ca^{2+} and the functional groups of the proteins, leading to the formation of a cross-linked network. In SPS-SDS, the viscosity of the protein was higher compared to that in DW, SPS, and SPS-Lignin, and this was more noticeable in the case of whey protein, albumin, and SBI. The formation of a gel-like phase due to cross-linking between the proteins, SDS, and Ca^{2+} is suggested as the reason for the increased viscosity of the proteins in SPS-SDS. The proteins demonstrated a similar viscosity in SPS and SPS-Lignin. The interfacial shear strength between the cement mortar surface and modified proteins was generally higher for proteins modified in SPS-SDS and SPS-Lignin compared to that in SPS only. The increased cross-linked bonds between the proteins and SDS or lignin is responsible for the higher interfacial shear strength. Modified NFMP in SPS-Lignin, however, showed a significant loss in the interfacial shear strength, and this was attributed to the complete hydrolysis of the NFMP molecular structure, which rendered the protein ineffective in forming strong networks. The cracked cement mortar prisms healed in various SBI solutions showed significantly higher flexural strength recovery after 7-day healing cycles, compared to the cracked prisms healed in SPS only. The cracked cement mortar prisms healed in SBI-SPS-SDS demonstrated the highest flexural strength recovery compared to other samples. The flexural strength recovery of the cracked cement mortar prisms was consistent with the interfacial shear strength test results. The optical and micro-CT analyses showed improved crack filling after the 7-day healing cycles in all cracked cement mortar prisms, with the prism healed in SBI-SPS-SDS showing relatively higher filling compared to the prisms healed in other media. The crack-filling observations seemed to be consistent with the flexural strength recovery results.

■ ASSOCIATED CONTENT

Supporting Information

The Supporting Information is available free of charge at https://pubs.acs.org/doi/10.1021/acsaenm.3c00423.

Schematic illustration of the interfacial strength test, image of the setup for the flexural strength recovery test, and schematic depicting the volume of the prisms used in micro-CT (PDF)

■ AUTHOR INFORMATION

Corresponding Author

Ali Ghahremaninezhad − *Department of Civil and Architectural Engineering, University of Miami, Coral Gables, Florida 33146, United States;* orcid.org/0000-0001-9269-801X; Phone: (+1) 305-2843465; Email: a.ghahremani@miami.edu

Author

Elvis Baffoe − *Department of Civil and Architectural Engineering, University of Miami, Coral Gables, Florida 33146, United States*

Complete contact information is available at: https://pubs.acs.org/10.1021/acsaenm.3c00423

Notes

The authors declare no competing financial interest.

■ ACKNOWLEDGMENTS

This study was supported in part by the National Science Foundation under the CAREER Award 1846984 and the Office of Naval Research under Award N00014221255. X-ray micro-CT imaging was made possible by the National Science Foundation under MRI Award 1920127. Any opinions, findings, and conclusions or recommendations expressed in this material are those of the author(s) and do not necessarily reflect the views of the National Science Foundation.

■ REFERENCES

(1) Espinosa, H. D.; Juster, A. L.; Latourte, F. J.; Loh, O. Y.; Gregoire, D.; Zavattieri, P. D. Tablet-level origin of toughening in abalone shells and translation to synthetic composite materials. *Nat. Commun.* **2011**, *2*. DOI: 10.1038/ncomms1172.

(2) Kim, Y. Y.; Carloni, J. D.; Demarchi, B.; Sparks, D.; Reid, D. G.; Kunitake, M. E.; Tang, C. C.; Duer, M. J.; Freeman, C. L.; Pokroy, B.; Penkman, K.; Harding, J. H.; Estroff, L. A.; Baker, S. P.; Meldrum, F. C. Tuning hardness in calcite by incorporation of amino acids. *Nat. Mater.* **2016**, *15*, 903–910.

(3) Baffoe, E.; Ghahremaninezhad, A. Effect of proteins on the mineralization, microstructure and mechanical properties of carbonation cured calcium silicate. *Cem Concr Compos.* **2023**, *141*, No. 105121.

(4) DeJong, J. T.; Fritzges, M. B.; Nüsslein, K. Microbially Induced Cementation to Control Sand Response to Undrained Shear. *Journal of Geotechnical and Geoenvironmental Engineering* **2006**, *132*, 1381–1392.

(5) Whiffin, V. S.; van Paassen, L. A.; Harkes, M. P. Microbial carbonate precipitation as a soil improvement technique. *Geomicrobiol J.* **2007**, *24*, 417–423.

(6) Chaturvedi, S.; Chandra, R.; Rai, V. Isolation and characterization of Phragmites australis (L.) rhizosphere bacteria from contaminated site for bioremediation of colored distillery effluent. *Ecol Eng.* **2006**, *27*, 202−207.
(7) Baffoe, E.; Ghahremaninezhad, A. The effect of biomolecules on enzyme-induced calcium carbonate precipitation in cementitious materials. *Constr. Build. Mater.* **2022**, *345*, 128323.
(8) De Muynck, W.; Verbeken, K.; De Belie, N.; Verstraete, W. Influence of urea and calcium dosage on the effectiveness of bacterially induced carbonate precipitation on limestone. *Ecol Eng.* **2010**, *36*, 99−111.
(9) Baffoe, E.; Ghahremaninezhad, A. On the interaction between proteins and cracked cementitious surface. *Constr Build Mater.* **2022**, *352*, No. 128982.
(10) Snoeck, D.; Van Tittelboom, K.; Steuperaert, S.; Dubruel, P.; De Belie, N. Self-healing cementitious materials by the combination of microfibres and superabsorbent polymers. *J. Intelligent Mater. Syst. Struct.* **2014**, *25*, 13.
(11) Jonkers, H.; Thijssen, A.; Muyzer, G.; Copuroglu, O.; Schlangen, E. Application of bacteria as self-healing agent for the development of sustainable concrete. *Ecol. Eng.* **2010**, *36*, 230−235.
(12) Belcher, A. M.; Wu, X. H.; Christensen, R. J.; Hansma, P. K.; Stucky, G. D.; Morse, D. E. Control of crystal phase switching and orientation by soluble mollusc-shell proteins. *Nature* **1996**, *381*, 56−58.
(13) Costa, O. Y. A.; Raaijmakers, J. M.; Kuramae, E. E. Microbial extracellular polymeric substances: Ecological function and impact on soil aggregation. *Front Microbiol.* **2018**, *9*, 1−14.
(14) Raydan, N. D. V.; Leroyer, L.; Charrier, B.; Robles, E. Recent advances on the development of protein-based adhesives for wood composite materials—a review. *Molecules* **2021**, *26*, 7617.
(15) Rong, H.; Qian, C. X. Binding functions of microbe cement. *Adv. Eng. Mater.* **2015**, *17*, 334−340.
(16) Brzyski, P.; Suchorab, Z.; Łagód, G. The influence of casein protein admixture on pore size distribution and mechanical properties of lime-metakaolin paste. *Buildings* **2021**, *11*, 530.
(17) Ventola, L.; Vendrell, M.; Giraldez, P.; Merino, L. Traditional organic additives improve lime mortars: New old materials for restoration and building natural stone fabrics. *Constr Build Mater.* **2011**, *25*, 3313−3318.
(18) Kamali, M.; Ghahremaninezhad, A. Effect of Biomolecules on the Nanostructure and Nanomechanical Property of Calcium-Silicate-Hydrate. *Sci. Rep.* **2018**, *8*, 1−16.
(19) Roberts, A.D.; Whittall, D.R.; Breitling, R.; Takano, E.; Blaker, J.J.; Hay, S.; Scrutton, N.S. Blood, sweat, and tears: extraterrestrial regolith biocomposites with in vivo binders. *Mater. Today Bio.* **2021**, *12*, 100136.
(20) Almajed, A.; Tirkolaei, H. K.; Kavazanjian, E.; Hamdan, N. Enzyme induced biocementated sand with high strength at low carbonate content. *Sci. Rep.* **2019**, *9*, 1−7.
(21) Pradyawong, S.; Qi, G.; Li, N.; Sun, X. S.; Wang, D. Adhesion properties of soy protein adhesives enhanced by biomass lignin. *Int. J. Adhes Adhes* **2017**, *75*, 66−73.
(22) Huang, W.; Sun, X. Adhesive Properties of Soy Proteins Modified by Sodium Dodecyl Sulfate and Sodium Dodecylbenzene Sulfonate. *J Am. Oil Chem. Soc.* **2000**, *77*, 705.
(23) Pye, E. K. Industrial Lignin Production and Applications. *Biorefineries—Industrial Processes and Products*; Wiley-VCH Verlag GmbH: Weinheim, Germany, 2005; pp 165−200. DOI: 10.1002/9783527619849.ch22.
(24) Xiao, Z.; Li, Y.; Wu, X.; Qi, G.; Li, N.; Zhang, K.; Wang, D.; Sun, X. S. Utilization of sorghum lignin to improve adhesion strength of soy protein adhesives on wood veneer. *Ind. Crops Prod.* **2013**, *50*, 501−509.
(25) Pradyawong, S.; Qi, G.; Zhang, M.; Sun, X. S.; Wang, D. Effect of pH and pH-shifting on adhesion performance and properties of lignin-protein adhesives. *Trans ASABE* **2021**, *64*, 1141−1152.
(26) Doherty, W. O. S.; Mousavioun, P.; Fellows, C. M. Value-adding to cellulosic ethanol: Lignin polymers. *Ind. Crops Prod.* **2011**, *33*, 259−276.
(27) Arriaga, T. V. Controlled and tailored denaturation and aggregation of whey proteins Tatiana Vieira Arriaga Engenharia Biológica Júri. Thesis, 2011.
(28) Shoulders, M. D.; Raines, R. T. Collagen structure and stability. *Annu. Rev. Biochem.* **2009**, *78*, 929−958.
(29) Singh, M. Structural interactions of globular proteins - Bovine serum albumin, egg albumin, and lysozyme, in aqueous medium, elucidated with molar volumes, viscosities, energy functions, and IR spectra from 293.15 to 303.15 K. *J. Appl. Polym. Sci.* **2007**, *103*, 1420−1429.
(30) Masoule, M. S. T.; Baffoe, E.; Ghahremaninezhad, A. On the physicochemical properties and foaming characteristics of proteins in cement environment. *Constr Build Mater.* **2023**, *366*, No. 130204.
(31) Pradyawong, S.; Qi, G.; Li, N.; Sun, X. S.; Wang, D. Adhesion properties of soy protein adhesives enhanced by biomass lignin. *Int, J. Adhes. Adhes.* **2017**, *75*, 66−73.
(32) Jafari, M.; Mehrnejad, F.; Rahimi, F.; Asghari, S. M. The Molecular Basis of the Sodium Dodecyl Sulfate Effect on Human Ubiquitin Structure: A Molecular Dynamics Simulation Study. *Sci. Rep.* **2018**, *8*, 1−15.
(33) Hansen, J. H.; Petersen, S. V.; Andersen, K. K.; Enghild, J. J.; Damhus, T.; Otzen, D. Stable intermediates determine proteins' primary unfolding sites in the presence of surfactants. *Biopolymers* **2009**, *91*, 221−231.
(34) Jiang, G.; Nowakowski, D. J.; Bridgwater, A. V. A systematic study of the kinetics of lignin pyrolysis. *Thermochim. Acta* **2010**, *498*, 61−66.
(35) Delaveau, J.; Jelen, P. Effect of pH on viscosity of sweet and acid wheys. *Dairy Sci.* **1979**, *62*, 1455−1457.
(36) Patil, S.; Sandberg, A.; Heckert, E.; Self, W.; Seal, S. Protein adsorption and cellular uptake of cerium oxide nanoparticles as a function of zeta potential. *Biomaterials* **2007**, *28*, 4600−4607.
(37) Zhang, Y.; Yang, M.; Portney, N. G.; Cui, D.; Budak, G.; Ozbay, E.; Ozkan, M.; Ozkan, C. S. Zeta potential: A surface electrical characteristic to probe the interaction of nanoparticles with normal and cancer human breast epithelial cells. *Biomed, Microdevices* **2008**, *10*, 321−328.
(38) Matsakas, L.; Karnaouri, A.; Cwirzen, A.; Rova, U.; Christakopoulos, P. Formation of lignin nanoparticles by combining organosolv pretreatment of birch biomass and homogenization processes. *Molecules* **2018**, *23*, 1822.
(39) Loosli, F.; Stoll, S. Effect of surfactants, pH and water hardness on the surface properties and agglomeration behavior of engineered TiO2 nanoparticles. *Environ, Sci. Nano.* **2017**, *4*, 203−211.
(40) Project, E.; Friedman, R.; Nachliel, E.; Gutman, M. A molecular dynamics study of the effect of Ca2+ removal on calmodulin structure. *Biophys. J.* **2006**, *90*, 3842−3850.
(41) Haris, P. I.; Severcan, F. FTIR spectroscopic characterization of protein structure in aqueous and non-aqueous media. *J. Mol. Catal. B Enzym.* **1999**, *7*, 207−221.
(42) Alhazmi, H.A. FT-IR spectroscopy for the identification of binding sites and measurements of the binding interactions of important metal ions with bovine serum albumin. *Sci. Pharm.* **2019**, *87*, 5.
(43) Cai, S.; Singh, B. R. A distinct utility of the amide III infrared band for secondary structure estimation of aqueous protein solutions using partial least squares methods. *Biochemistry* **2004**, *43*, 2541−2549.
(44) Anderle, G.; Mendelsohn, R. Thermal denaturation of globular proteins. Fourier transform-infrared studies of the amide III spectral region. *Biophys. J.* **1987**, *52*, 69−74.
(45) Kizil, R.; Irudayaraj, J.; Seetharaman, K. Characterization of irradiated starches by using FT-Raman and FTIR spectroscopy. *J. Agric. Food Chem.* **2002**, *50*, 3912−3918.
(46) Zhan, F.; Hu, J.; He, C.; Sun, J.; Li, J.; Li, B. Complexation between sodium caseinate and gallic acid: Effects on foam properties

and interfacial properties of foam. *Food Hydrocoll* **2020**, *99*, No. 105365.
(47) Zhan, F.; Yang, J.; Li, J.; Wang, Y.; Li, B. Characteristics of the interaction mechanism between tannic acid and sodium caseinate using multispectroscopic and thermodynamics methods. *Food Hydrocoll.* **2018**, *75*, 81−87.
(48) Xu, Y. Y.; Xu, Y. Y.; Zhu, W.; Zhang, W.; Gao, Q.; Li, J. Improve the performance of soy protein-based adhesives by a polyurethane elastomer. *Polymers (Basel)* **2018**, *10*, 1016.
(49) Qi, G.; Sun, X. S. Soy protein adhesive blends with synthetic latex on wood veneer. *J Am. Oil Chem. Soc.* **2011**, *88*, 271−281.
(50) Kwon, H.; Squire, C. J.; Young, P. G.; Baker, E. N. Autocatalytically generated Thr-Gln ester bond cross-links stabilize the repetitive Ig-domain shaft of a bacterial cell surface adhesin. *Proc. Natl. Acad. Sci. U. S. A.* **2014**, *111*, 1367−1372.
(51) Master, A. M.; Rodriguez, M. E.; Kenney, M. E.; Oleinick, N. L.; Gupta, A. S. Delivery of the photosensitizer Pc 4 in PEG−PCL micelles for in vitro PDT studies. *J. Pharm. Sci.* **2010**, *99*, 2386−2398.
(52) Wang, X.; He, Z.; Zeng, M.; Qin, F.; Adhikari, B.; Chen, J. Effects of the size and content of protein aggregates on the rheological and structural properties of soy protein isolate emulsion gels induced by CaSO4. *Food Chem.* **2017**, *221*, 130−138.
(53) Sandra, S.; Ho, M.; Alexander, M.; Corredig, M. Effect of soluble calcium on the renneting properties of casein micelles as measured by rheology and diffusing wave spectroscopy. *J, Dairy Sci.* **2012**, *95*, 75−82.
(54) Walnofer, R. S.; Hettiarachchy, N. S.; Horax, R. Effects of heating on hydrophobicity, viscosity, and gelling properties of soy products. *Discovery* **2005**, *6*, 38−44.
(55) Roversi, M.; La Mesa, C. Rheological properties of protein-surfactant based gels. *J. Colloid Interface Sci.* **2005**, *284*, 470−476.
(56) Luo, J.; Luo, J.; Yuan, C.; Zhang, W.; Li, J.; Gao, Q.; Chen, H. An eco-friendly wood adhesive from soy protein and lignin: performance properties. *RSC Adv.* **2015**, *5*, 100849−100855.
(57) Dissanayake, M.; Vasiljevic, T. Functional properties of whey proteins affected by heat treatment and hydrodynamic high-pressure shearing. *J. Dairy Sci.* **2009**, *92*, 1387−1397.
(58) De Wit, J. N. Thermal stability and functionality of whey proteins. *J. Dairy Sci.* **1990**, *73*, 3602−3612.
(59) Paulsson, M.; Dejmek, P. Thermal denaturation of whey proteins in mixtures with caseins studied by differential scanning calorimetry. *J. Dairy Sci.* **1990**, *73*, 590−600.
(60) Patel, M. T.; Kilara, A.; Huffman, L. M.; Hewitt, S. A.; Houlihan, A. V. Studies on whey protein concentrates. 1. compositional and thermal properties. *J. Dairy Sci.* **1990**, *73*, 1439−1449.
(61) Gujar, P.; Murali, N.; Ilango, N. K.; Santhanam, M.; Ghosh, P. Engineering interfacial strength of polymer coated hydrating cement paste by tuning calcium characteristics. *Mater. Struct.* **2023**, *56*, 1−18.
(62) Salas, C.; Rojas, O. J.; Lucia, L. A.; Hubbe, M. A.; Genzer, J. On the surface interactions of proteins with lignin. *ACS Appl. Mater. Interfaces* **2013**, *5*, 199−206.
(63) Snoeck, D.; De Belie, N. Mechanical and self-healing properties of cementitious composites reinforced with flax and cottonised flax, and compared with polyvinyl alcohol fibres. *Biosyst Eng.* **2012**, *111*, 325−335.
(64) Mignon, A.; Vermeulen, J.; Snoeck, D.; Dubruel, P.; Van Vlierberghe, S.; De Belie, N. Mechanical and self-healing properties of cementitious materials with pH-responsive semi-synthetic superabsorbent polymers. *Mater. Structures/Materiaux et Constructions* **2017**, *50*. DOI: 10.1617/s11527-017-1109-4.
(65) Utay, N. S.; Asmuth, D. M.; Gharakhanian, S.; Contreras, M.; Warner, C. D.; Detzel, C. J. Potential use of serum-derived bovine immunoglobulin/protein isolate for the management of COVID-19. *Drug Dev Res.* **2021**, *82*, 873−879.
(66) Galliano, A.; Bistac, S.; Schultz, J. Adhesion and friction of PDMS networks: Molecular weight effects. *J, Colloid Interface Sci.* **2003**, *265*, 372−379.
(67) Martin, K.; Tirkolaei, H.K.; Kavazanjian, E. Enhancing the strength of granular material with a modified enzyme-induced carbonate precipitation (EICP) treatment solution. *Constr Build Mater.* **2021**, *271*, 121529.
(68) Huang, W.; Sun, X. Adhesive properties of soy proteins modified by urea and guanidine hydrochloride. *J Am. Oil Chem. Soc.* **2000**, *77*, 101−104.

https://doi.org/10.1021/acsaenm.3c00423
ACS Appl. Eng. Mater. 2023, 1, 2685−2697